Frontiers in Bioscience Landmark

Front. Biosci. (Landmark Ed) **2026**; 31(1): 47028
https://doi.org/10.31083/FBL47028

Original Research

Mechanisms of Bellidifolin in Treating Doxorubicin-Induced Cardiotoxicity: Network Pharmacology, Molecular Docking, and Experimental Verification

Xinmeng Zhao[1,2,3,†], Zhenyang Zhong[1,2,3,†], Fan Gao[3], Jiangli Wu[2,3], Cheng Dai[1,2,3], Yalei Liu[1], Yu Liu[1,2,3,*], Aiying Li[1,2,3,*]

[1]Department of Biochemistry and Molecular Biology, College of Pharmacy, Hebei University of Chinese Medicine, 050200 Shijiazhuang, Hebei, China
[2]Hebei Key Laboratory of Chinese Medicine Research on Cardio-cerebrovascular Disease, 050091 Shijiazhuang, Hebei, China
[3]Hebei Higher Education Institute Applied Technology Research Center on TCM Development and Industrialization, 050091 Shijiazhuang, Hebei, China
*Correspondence: liuyu000252@hebcm.edu.cn (Yu Liu); liaiying@hebcm.edu.cn (Aiying Li)
[†]These authors contributed equally.
Academic Editor: Vesna Jacevic
Submitted: 29 September 2025 Revised: 5 December 2025 Accepted: 19 December 2025 Published: 21 January 2026

Abstract

Background: This study aims to examine the roles and mechanisms of action of bellidifolin (BEL) in alleviating doxorubicin-mediated cardiotoxicity using network pharmacology and experimental validation . **Materials and Methods**: Mice with doxorubicin-induced cardiotoxicity were randomly assigned to control, model, BEL, and dexrazoxane (DEX) groups. Echocardiography, histological staining, network pharmacology, and molecular validation were employed to assess cardiac function and myocardial injury. Immunohistochemical staining, western blotting, and RT-qPCR were used to confirm predicted targets and fibrosis biomarkers. **Results**: *In vivo* experiments demonstrated that BEL significantly improved cardiac function, as indicated by enhanced Ejection Fraction (EF) and Fractional Shortening (FS) compared to the model group ($p < 0.01$). BEL also notably reduced myocardial injury markers, including creatine kinase MB isoenzyme (CK-MB) and lactate dehydrogenase (LDH) ($p < 0.01$), and alleviated doxorubicin-induced myocardial fibrosis. Network pharmacology identified 61 common target genes for BEL and cardiotoxicity. Proteinprotein interaction (PPI) network analysis highlighted 16 core genes, including transforming growth factor (TGF)-β1. Kyoto Encyclopedia of Genes and Genomes (KEGG) and Gene Ontology (GO) enrichment analyses revealed that BEL's action pathways were primarily linked to the PI3K-AKT signaling pathway. Molecular docking and dynamic simulations showed a strong binding affinity between BEL and the core target TGF-β1. *In vivo* validation confirmed that BEL significantly downregulated the expression of TGF-β1, α-smooth muscle actin (SMA), collagen I (Col I), and collagen III (Col III) in myocardial tissue ($p < 0.01$ or $p < 0.05$), while activating the PI3K-AKT signaling pathway ($p < 0.01$ or $p < 0.05$). **Conclusion**: BEL presents as a promising therapeutic candidate for cardiotoxicity, likely through its anti-fibrotic effects via the reduction of TGF-β1, α-SMA, Col I, and Col III expression, alongside regulation in the PI3K-AKT signaling pathway.

Keywords: doxorubicin; cardiotoxicity; endomyocardial fibrosis; network pharmacology; molecular dynamics simulation

1. Introduction

Doxorubicin (DOX) is a widely used antibiotic for treating various malignant tumors [1]. While DOX is highly effective in its antitumor and antibacterial properties, increasing evidence highlights its potential cardiotoxicity [2]. DOX-induced cardiotoxicity (DIC) commonly manifests as myocardial cell damage, fibrosis, and cardiac insufficiency, which may progress to heart failure, significantly impacting patient quality of life and prognosis [3]. The pathological mechanisms underlying DIC involve a cascade of molecular events, including excessive oxidative and nitrosative stress, mitochondrial dysfunction, apoptosis, impaired autophagy, and the dysregulation of key signaling pathways such as AMPK, Nrf2, TGF-β1/Smad2, and HIF-1α. Additionally, epigenetic alterations contribute to myocardial injury [4]. Currently, drugs used for the clinical prevention and treatment of DIC, such as Dexrazoxane (DEX), have limitations in efficacy and associated side effects [5]. Furthermore, DEX's potential adverse reactions include a reduction in the antitumor efficacy of anthracyclines and the development of secondary malignancies, particularly in children [6]. Thus, identifying drugs that can effectively alleviate DOX-induced cardiotoxicity is critical to improving clinical outcomes and reducing mortality in cancer patients.

In Inner Mongolia, *Gentianella acuta* (*G. acuta*) is commonly used as a medicinal tea for preventing cardiovascular diseases [7]. As documented in the Mongolian Herbal Medicine Records, *G. acuta* is traditionally used to treat conditions such as angina pectoris, jaundice, and cholecystitis, and it is widely employed in clinical practice to alleviate myocardial fibrosis and cardiovascular injury [8–12]. Bellidifolin (BEL), an active xanthone molecule derived from *G. acuta*, has the molecular formula $C_{14}H_{10}O_6$ and a molecular weight of 274.22 g/mol [13]. Previous studies

Copyright: © 2026 The Author(s). Published by IMR Press.
This is an open access article under the CC BY 4.0 license.

Publisher's Note: IMR Press stays neutral with regard to jurisdictional claims in published maps and institutional affiliations.

have demonstrated that BEL can mitigate myocardial fibrosis through multiple mechanisms [14,15].

Network pharmacology, based on systems biology principles, analyzes biological networks to identify signal nodes for multi-target drug design [16]. Molecular docking and molecular dynamics simulations can verify the binding modes and interaction strengths between drugs and targets at the molecular level. Combined with *in vivo* experiments, these methods offer an efficient approach to elucidating the pharmacodynamic basis of natural products [17]. While prior studies confirmed BEL's role in improving myocardial fibrosis, its specific molecular mechanism remains unclear. Based on bioinformatics, BEL's therapeutic effect may be associated with the fibrosis-related target TGF-β1. To test this hypothesis, the present study utilizes a DIC mouse model to identify the potential targets and pathways of BEL in treating DIC through network pharmacology, confirm the binding activity of core targets and BEL using molecular docking, and systematically validate BEL's protective effect and molecular mechanism *in vivo*. The study aims to provide a theoretical foundation for developing BEL as a therapeutic drug for DIC, while broadening the application of natural products in the prevention and treatment of chemotherapy-induced cardiotoxicity.

2. Materials and Methods

2.1 Drug Preparation

BEL (Lot: AFDE3105, Purity: 98%, Chengdu Alfa Biotechnology Co., Ltd., China) was used in this study. In the preliminary experiment, two gradient doses of BEL (25 mg/(kg·d) and 50 mg/(kg·d)) were selected based on literature data for similar drugs and species-equivalent dose conversion standards. Pharmacodynamic observations of cardiac function and myocardial injury indicators revealed that the cardioprotective effect of BEL was dose-dependent. Thus, 50 mg/(kg·d) was chosen for further investigation [14,15]. Based on previous research and references, DOX (Lot: NO.2541019001, Beijing Solarbio Science & Technology Co., Ltd., China) was administered at a dose of 5 mg/kg [14,15,18]. DEX (Lot: J14IS219829, Shanghai Yuanye Bio-Technology Co., Ltd., China), a Food and Drug Administration (FDA)-approved drug used to prevent DOX-induced cardiotoxicity in high-risk patients, was included as a positive control at a dose of 50 mg/kg, which is 10 times the DOX dose. This dose was chosen to ensure the accuracy and reliability of the results [5,19].

2.2 Animal Grouping and Administration

Sixty specific-pathogen-free (SPF) male C57BL/6 mice (8 weeks old, body weight 18–22 g) were obtained from Beijing Sibeifu Biotechnology Co., Ltd. (License No.: SCXK (Beijing) 2019-0010). All mice were housed individually in cages with free access to food and water, in a well-ventilated environment with a 12-hour light/dark cycle, a temperature of 20–25 °C, and relative humidity maintained at 40%–70%. The experiment was approved by the Animal Welfare Committee of Hebei University of Chinese Medicine (Approval No.: DWLL202212032).

The mice were randomly divided into four groups (15 mice per group) using a random number table: Control, Model, BEL, and DEX groups. The Model, BEL, and DEX groups were intraperitoneally injected with 5 mg/kg DOX to establish a myocardial injury model, while the Control group received the same dose of normal saline via intraperitoneal injection once a week for 4 weeks. Echocardiography and myocardial tissue pathological staining were used to assess the success of modeling. In addition to DOX injection, the BEL group received 50 mg/(kg·d) of BEL monomer suspension via intragastric administration for 28 consecutive days, while the DEX group was intraperitoneally injected with 50 mg/kg of DEX solution once a week for 4 weeks. The Control group was intragastrically administered normal saline at the same dose for 28 days.

2.3 Efficacy Verification of BEL in Treating Doxorubicin-Induced Cardiotoxicity

2.3.1 Observation of General Status of Mice

Throughout the experiment, the mice's mental state, activity levels, water intake, and food intake were observed and recorded daily. Body weight measurements were taken weekly to adjust the gavage volume accordingly.

2.3.2 Electrocardiogram (ECG) and Echocardiography Detection

ECG detection: After drug administration, mice were anesthetized via intraperitoneal injection of pentobarbital sodium (For sodium pentobarbital: It was prepared into a 3% solution using sterile normal saline, and administered via intermittent and slow intraperitoneal injection at a standard dose of 50 mg/kg body weight). Afterward, they were placed supine on the experimental platform, and their extremities were subcutaneously linked to the BL-420S biological function experimental system. The standard lead II ECG was monitored for 60–120 seconds.

Echocardiography detection: The evaporator of the anesthesia machine was connected to an air pump, with the output gas flow rate set at 300–500 mL/min. Mice were placed in an anesthesia induction chamber with 3–4% isoflurane until fully anesthetized (approximately 2–3 minutes). Once the mice were fully anesthetized, the concentration was reduced to a maintenance level of 1–1.5%. The mice were removed from the induction chamber, their heads and noses fixed in an anesthetic mask, and positioned supine on the detection table with limbs attached to electrode pads. After depilating the chest, the ultrasonic probe was placed closely against the mice's chest wall. Cardiac ultrasound was performed using a small animal ultrasound imaging system, where Left Ventricular Posterior Wall thickness in systole (LVPWs), Left Ventricular Poste-

rior Wall thickness in diastole (LVPWd), Left Ventricular Volume in systole (LVVols), Left Ventricular Volume in diastole (LVVold), Left Ventricular Internal Diameter in systole (LVIDs), Left Ventricular Internal Diameter in diastole (LVIDd), Fractional Shortening (FS), and Ejection Fraction (EF) were measured. Turn off the evaporator after the procedure is completed, and the mice were kept breathing pure oxygen for approximately 5–10 minutes to facilitate their rapid recovery.

2.3.3 Sample Collection

After completing the ECG and echocardiography, the mice were fasted for 12 hours with free access to water. Blood was collected via eyeball enucleation into clean test tubes, and serum was separated by centrifugation. The supernatant was stored at –80 °C for subsequent biomarker assays. The operator pressed the mouse's head and neck with the thumb and index finger, while grasping the mouse's tail or hind limbs with the other hand. Then, the operator quickly pulled the hindquarters backward and upward with force to dislocate the cervical vertebrae. The chest cavity was then rapidly opened, and a 1.0 mm × 1.0 mm sample of cardiac tissue was excised from the apex, immersed in electron microscopy fixative, and kept at room temperature for 2 hours before being stored at 4 °C for ultrastructural analysis of myocardial mitochondria and microvessels. Another portion of cardiac tissue was fixed in 4% paraformaldehyde, with a suitable-sized sample frozen in cryotubes at –80 °C for pathological morphology observation and gene/protein expression analysis.

2.3.4 Body Weight and Heart Weight Measurement

After 4 weeks of administration, the mice's body weight was recorded, and the abdomen was incised to expose the heart. The abdominal aorta was ligated, and residual blood in the heart was flushed with pre-cooled saline. The tissue was blotted dry with filter paper before weighing to record heart weight.

2.3.5 HE Staining and Masson Staining to Observe Pathological Morphological Changes of Heart Tissue

Heart tissues were fixed with 4% paraformaldehyde (G1101, Wuhan Servicebio Technology Co., Ltd., Wuhan, China), processed through routine paraffin embedding, sectioned, and stained with HE and Masson. Pathological alterations in myocardial tissue were examined microscopically.

2.3.6 Sirius Red Staining to Detect the Degree of Myocardial Cell Fibrosis in Mice

The heart tissue of the mice was stained with Sirius red to assess fibrotic changes in the myocardial tissue under a microscope. ImageJ 1.51j software (National Institutes of Health, Bethesda, MD, USA) was used for quantitative analysis of the collagen area, allowing evaluation of the degree of fibrosis.

2.3.7 Biochemical Method to Detect the Contents of Serum LDH, CK-MB, ALT, UREA, and CREA

Following serum collection, the levels of LDH (lactate dehydrogenase), CK-MB (creatine kinase MB isoenzyme), ALT (alanine aminotransferase), UREA (urea), and CREA (creatinine) were measured using an automatic biochemical analyzer (Chemray 800, Rayto Life and Analytical Sciences Co., Ltd., Shenzhen, Guangdong, China).

2.4 Network Pharmacology Study

2.4.1 Determination of Main Action Targets of BEL

Target identification for BEL involved retrieving data from multiple sources, including Traditional Chinese Medicine Systems Pharmacology Database and Analysis Platform (TCMSP, https://www.tcmsp-e.com/load_intro.php?id=43), Traditional Chinese Medicine Integrated Database (TCMID, https://bidd.group/TCMID/), and other chemical databases (Chemical professional database, http://www.organchem.csdb.cn/scdb/default.asp). The 3D structure and Canonical Simplified Molecular Input Line Entry System (SMILES) of BEL were obtained from PubChem (https://pubchem.ncbi.nlm.nih.gov/) and used in the Swiss Target Prediction database (http://www.swisstargetprediction.ch/) for further exploration. After eliminating duplicate targets, species were restricted to "Homo sapiens" using the UniProt database (https://www.uniprot.org/), and the target names were standardized into gene names to build the BEL target database.

2.4.2 Collection of Targets Related to DIC

For disease-related target identification, keywords like "cardiotoxicity", "anthracycline-induced cardiotoxicity", and "doxorubicin-induced cardiotoxicity" were used to retrieve targets from the GeneCards database (https://www.genecards.org/), with a relevance score cutoff of $\geq$1.0. Additionally, disease targets were sourced from the OMIM (http://www.omim.org/), DrugBank (https://go.drugbank.com/), and Genetic Association Database (GAD, https://maayanlab.cloud/Harmonizome/resource/Genetic+Association+Database), with gene names standardized in the UniProt database. After merging the search results and removing targets with duplicate or missing UniProt IDs, the final list of cardiotoxicity-related targets was obtained.

2.4.3 Screening of Key Targets of BEL in Treating Cardiotoxicity

The intersection of BEL targets and cardiotoxicity-related targets was extracted, representing the potential action targets of BEL in treating cardiotoxicity. These targets were imported into the STRING database (https://string-db.org/) for PPI analysis, selecting the "multiple pro-

teins" mode with the species limited to "Homo sapiens" and a confidence score of $\geq$0.4. The PPI interaction information was downloaded and saved as a TSV file. This file was then imported into Cytoscape 3.7.2 (Cytoscape Consortium, San Diego, CA, USA) for network topology analysis using the Analyze Network plug-in. The parameters Degree, Closeness, and Betweenness were used to evaluate the topological properties of each node. Nodes with higher values for these parameters were considered more important in the network. Targets with Degree, Closeness, and Betweenness above the average threshold were selected as key targets identified through network pharmacology.

2.4.4 GO and KEGG Pathway Analyses

Further functional analyses, including GO and KEGG enrichment analyses, were performed to explore the main biological functions and signaling pathways involved in the treatment of DIC by BEL. The targets were input into the DAVID 2021 platform (https://davidbioinformatics.nih.gov/) for biological information annotation, with "OFFICIAL_GENE_SYMBOL" as the identifier, "gene list" as the list type, and "Homo sapiens" as the species. The threshold was set at $p < 0.01$, and the results were visualized using the Bioinformatics online platform.

2.5 Molecular Docking

As a ligand, the 2D structure of compound BEL was retrieved from the PubChem database and stored in "sdf" format. For selecting PDB files of core gene-related proteins, the RCSB PDB database (https://www.rcsb.org/) was utilized, with the following selection criteria: experimental method—X-ray crystallography (the primary method for determining protein tertiary structures), target species—Homo sapiens (human-derived proteins were chosen to accurately represent *in vivo* structural characteristics and avoid binding mode discrepancies due to species differences), resolution—0.5–2.5 Å (proteins with a resolution within this range provide detailed information on amino acid side chains and hydrogen bond networks, ensuring docking accuracy), presence of ligands in the structure (facilitating direct identification of the docking region and minimizing invalid structures without target pockets), pH range—7.35–7.50 (representing the physiological pH of the human body, simulating the native conformation of proteins *in vivo*). The proteins were screened according to these criteria and stored in "PDB" format. The online molecular docking software CB-Dock2 (https://cadd.labshare.cn/cb-dock2/php/blinddock.php) was then used to evaluate the binding activity between the compound and the target gene. In the molecular docking results, a Vina score lower than –5 kJ/mol indicates good docking between the protein and the ligand, with a lower Vina score reflecting a more stable ligand-receptor binding.

2.6 Molecular Dynamics Simulation

Based on the molecular docking results, YASARA 10.3.16 (YASARA Bioinformatics GmbH, Vienna, Austria) was used for molecular dynamics simulations. The protonation state of the residues was corrected by adding hydrogens and optimizing bond lengths and angles. Periodic boundary conditions (PBC) were applied, counterions were added to neutralize the system, and the physiological pH was set to 7.4. The appropriate force field was selected for the simulation. Through energy minimization and equilibrium simulations, steric clashes between atoms were resolved, and the energy of the initial structure was minimized. The predefined MD macro file was executed, and equilibrium simulations in the canonical ensemble (NVT) and isothermal-isobaric ensemble (NPT) were conducted for 100 ps each, at a temperature of 298 K and a pressure of 1 bar. Subsequently, a 100 ns molecular dynamics simulation of the complex system was performed, with conformations saved every 10 ps. Using YASARA's built-in tools, parameters such as RMSD and RMSF were calculated to assess system stability. The binding free energy between the ligand and receptor was analyzed, and key interaction residues were identified through binding energy decomposition.

2.7 In Vivo Verification of Targets of BEL in Treating Cardiotoxicity

2.7.1 Immunohistochemistry to Detect the Expression Levels of TGF-β1, α-SMA, Col I, Col III in Myocardial Tissue

Paraffin sections prepared as described in section 1.5 were subjected to sequential dewaxing, hydration, and antigen retrieval. After a 3% hydrogen peroxide treatment to block endogenous peroxidase activity, the sections were sealed. The primary antibodies targeting TGF-β1 (1:20,000, 81746-2-RR, Proteintech Group, Inc, Wuhan, China), α-SMA (1:5000, 14395-1-AP, Proteintech Group, Inc, Wuhan, China), Col I (1:1000, HA722517, Hangzhou Huan Biotechnology Co., Ltd., Hangzhou, China), and Col III (1:1000, HA720050, Hangzhou Huan Biotechnology Co., Ltd., Hangzhou, China) were applied, and the sections were incubated overnight at 4 °C. The following day, horseradish peroxidase-conjugated secondary antibodies (G1267, Wuhan Servicebio Technology Co., Ltd., Wuhan, China) were applied at room temperature, followed by DAB development, hematoxylin counterstaining, image capture, and statistical analysis.

2.7.2 RT-qPCR to Detect the Gene Expression Levels of TGF-β1, α-SMA, Col I, Col III in Myocardial Tissue

The TRIzol method was utilized for the extraction of total RNA from mouse myocardial tissue, and cDNA was synthesized through reverse transcription. Real-time quantitative PCR was performed using SYBR qPCR Master Mix (G3325, Wuhan Servicebio Technology Co., Ltd., Wuhan, China), with primer sequences presented in Ta-

Table 1. Primer sequence.

Primer		Sequence (5′-3′)	Length/bp	Annealing Temperature
TGF-β1	Forward	ACTGGAGTTGTACGGCAGTG	121	60 °C
	Reverse	GGCTGATCCCGTTGATTTCC		
α-SMA	Forward	TCAGGGAGTAATGGTTGGAATG	348	60 °C
	Reverse	CCAGAGTCCAGCACAATACCAG		
Col I	Forward	GAGAGGTGAACAAGGTCCCG	153	60 °C
	Reverse	AAACCTCTCTCGCCTCTTGC		
Col III	Forward	GTGGCAATGTAAAGAAGTCTCTGAAG	191	60 °C
	Reverse	GGGTGCGATATCTATGATGGGTAG		
M-GAPDH	Forward	CCTCGTCCCGTAGACAAAATG	133	60 °C
	Reverse	TGAGGTCAATGAAGGGGTCGT		

TGF-β1, transforming growth factor-β1; α-SMA, α-smooth muscle actin; Col I, collagen I; Col III, collagen III; M-GAPDH, Mouse Glyceraldehyde-3-phosphate Dehydrogenase.

ble 1. The PCR program included pre-denaturation at 95 °C for 30 seconds, followed by 40 cycles of denaturation at 95 °C (10 seconds), annealing at a temperature ranging from 55 to 65 °C (10 seconds), and extension at 72 °C (30 seconds). Glyceraldehyde-3-phosphate dehydrogenase (GAPDH) acted as the internal control gene, and relative gene expression was determined using the $2^{-\Delta\Delta Ct}$ method.

2.7.3 WB to Detect the Gene Expression Levels of TGF-β1, α-SMA, Col I, Col III, PI3K and AKT in Myocardial Tissue

Radio Immunoprecipitation Assay (RIPA) lysis buffer (G2002, Wuhan Servicebio Technology Co., Ltd., Wuhan, China) was utilized for the lysis of myocardial tissue, and centrifugation was performed to harvest the supernatant. A BCA assay kit (G2026, Wuhan Servicebio Technology Co., Ltd., Wuhan, China) was used to determine the protein concentration. After separating protein samples by SDS-PAGE, they were transferred onto PVDF membranes. The membranes were blocked in 5% non-fat milk, incubated with primary antibodies (TGF-β1, 1:20,000, 81746-2-RR, Proteintech Group, Inc, Wuhan, China; α-SMA, 1:5000, 14395-1-AP, Proteintech Group, Inc, Wuhan, China; Col I, 1:1000, HA722517, Hangzhou Huan Biotechnology Co., Ltd., Hangzhou, China; Col III, 1:1000, HA720050, Hangzhou Huan Biotechnology Co., Ltd., Hangzhou, China) at 4 ℃ for 12–16 hours, and then incubated with horseradish peroxidase-conjugated secondary antibodies (G2009, Wuhan Servicebio Technology Co., Ltd., Wuhan, China). Protein signals were visualized using ECL solution, and quantification was conducted with ImageJ software.

2.8 Statistical Methods

Statistical analysis was conducted using SPSS 27.0 (IBM Corp., Chicago, IL, USA), while GraphPad Prism 8.0.2 (GraphPad Software, San Diego, CA, USA) was used to generate statistical graphs. Data normality was tested, and comparisons of normally distributed data were performed using one-way analysis of variance (ANOVA). For homogeneous variances, post-hoc testing was done using the least significant difference (LSD) method. For heterogeneous variances, the Dunnett's T3 test was applied. Data are presented as mean $\pm$ standard deviation ($\bar{x} \pm s$), and a p-value < 0.05 was considered statistically significant.

3. Results

3.1 BEL Effectively Improves Cardiac Function, Myocardial Injury, and Hepatorenal Damage in Cardiotoxic Mice

During the experiment, compared to the blank control group, mice in the model group exhibited reduced water and food intake, yellowing fur, and lethargy, among other symptoms. These conditions improved to varying degrees in the treatment groups when compared to the model group. Echocardiography results revealed that the cardiac contour and internal structure in the blank control group were normal, with the ventricular wall showing a regular contraction/relaxation rhythm. In contrast, the model group displayed left heart enlargement, abnormal ventricular wall motion, and decreased EF and FS, along with increased values of LVIDs, LVPWs, LVVols, LVIDd, LVPWd, and LVVold ($p < 0.01$). Each treatment group displayed significant improvement when compared with the model group ($p < 0.05$ or $p < 0.01$) (Fig. 1A,B). ECG results indicated that mice in the blank control group exhibited regular heart rhythms, while the model group showed arrhythmia, ST-segment depression, and other abnormalities. These issues improved to varying degrees in the treatment groups (Fig. 1C). The HW/BW% (heart weight-to-body weight ratio) in the model group was significantly elevated ($p < 0.01$), but the HW/BW% values in the treatment groups were significantly reduced ($p < 0.01$) (Fig. 1D). Indices of myocardial injury indicated that the levels of LDH and CK-MB were markedly increased in the model group in comparison with the control group ($p < 0.01$). In contrast, the treatment groups exhibited significant reductions in these

levels compared to the model group ($p < 0.05$ or $p < 0.01$) (Fig. 1E). Additionally, compared with the control group, the model group showed a significant decrease in the liver and kidney injury marker ALT ($p < 0.01$), while UREA and CREA levels were significantly increased ($p < 0.01$); after BEL treatment, UREA and CREA levels in mice decreased to varying degrees ($p < 0.05$ or $p < 0.01$), and CREA levels in the DEX group mice also showed a significant decrease ($p < 0.01$) (Fig. 1F).These results indicate that DOX induces significant damage to cardiac and hepatorenal functions in mice, while BEL effectively mitigates this damage.

3.2 BEL Ameliorates Pathological Changes in the Myocardium, Liver, and Kidney of Cardiotoxic Mice

Myocardial HE staining results (Fig. 2A,B) revealed that, compared to the control group, mice in the model group exhibited varying degrees of eosinophilic changes, marked swelling of myocardial cells, significant rupture of myocardial striations, fibroblast proliferation, considerable thickening of myocardial cells compared to normal cells, deep-stained cytoplasm, pyknosis of myocardial cell nuclei, progressive nuclear disappearance, and visible apoptosis and necrosis, accompanied by inflammatory cell infiltration in necrotic areas. In contrast, each treatment group showed significant improvements compared to the model group.

Liver HE staining results (Fig. 2C,D) indicated that liver tissue from mice in the model group exhibited extensive inflammatory cell infiltration around the portal vein, dilation of hepatic lobular venous lumens, and liver damage. The inflammatory infiltration in liver tissue was markedly reduced in all treatment groups compared to the model group.

Kidney HE staining results (Fig. 2E,F) showed that compared to the control group, renal tissue in the model group exhibited obvious tubular epithelial edema, swollen cells, vacuolated cytoplasm, visible connective tissue hyperplasia, and lymphocyte infiltration. Pathological damage in the renal tissue was significantly alleviated in all treatment groups compared to the model group.

To further assess myocardial injury, the microstructure of the mouse myocardium was observed by transmission electron microscopy (TEM). As shown in Fig. 2G,H, myocardial mitochondria in the blank control group were neatly arranged, numerous, with intact mitochondrial membrane structures, clear cristae, and no rupture or obvious hypertrophy. In contrast, myocardial mitochondria in the model group were disorganized, condensed, scattered, with dissolution and disappearance of surrounding myofilaments, mitochondrial cristae rupture, hypertrophy, hyperplasia, and severe vacuolization. The administration groups showed significant improvements in mitochondrial structure compared to the model group.

3.3 BEL Ameliorates Myocardial Fibrosis in Cardiotoxic Mice

Myocardial Masson staining results (Fig. 3A,B) revealed that myocardial cells appeared pink, while collagen fibers were stained blue-purple. Compared to the blank control group, myocardium in the other groups exhibited varying degrees of injury. In the model group, pathological sections showed disorganized myocardial cell arrangement, significant accumulation of blue-purple fibrous collagen, and destruction of myocardial structure. In contrast, the administration groups exhibited more organized myocardial cells with reduced collagen fiber accumulation compared to the model group. The Masson staining results indicated a strong correlation between cardiotoxicity and the development of myocardial fibrosis. To further assess collagen expression in myocardial tissues, Sirius red staining and Sirius red polarized light staining were performed. The results were consistent with the Masson staining, showing that collagen expression in myocardial tissues correlated with the severity of fibrosis, as shown in Fig. 3C–F.

3.4 Mechanistic Prediction of BEL Intervention in Doxorubicin-Induced Cardiotoxicity

3.4.1 Screening of Potential Targets for BEL Intervention in Doxorubicin-Induced Cardiotoxicity

After merging and removing duplicates from the collected targets, the targets were imported into the UniProt database for standardization. A total of 180 targets corresponding to BEL and 1478 targets related to DIC were retrieved. The intersection of these targets resulted in 61 potential targets for BEL in the treatment of DIC, as shown in Fig. 4A.

3.4.2 Screening of Key Targets for BEL Intervention in Doxorubicin-Induced Cardiotoxicity

As depicted in Fig. 4B, the PPI network of BEL interfering with DOX-induced cardiotoxicity contained 66 nodes and 828 edges, where nodes represented proteins and edges denoted their mutual relationships. Targets with Degree, Closeness, and Betweenness values higher than the average were identified as key targets for BEL intervention in DIC. The specific details of all targets are presented in Table 2.

3.4.3 GO Biological Function Analysis

GO functional annotation analysis ($p \leq 0.01$) was performed on 16 key targets of BEL intervention in DIC, identifying 246 biological function entries. Of these, 199 were related to biological processes (BP), 26 to molecular functions (MF), and 21 to cellular components (CC), accounting for 81%, 10.5%, and 8.5% of the total, respectively. Secondary classification annotation was conducted for each GO entry, as shown in Fig. 4C. The top 5 BP, CC, and MF entries were selected in ascending order of p-values for visualization in Fig. 4D. The size of the circles represents the

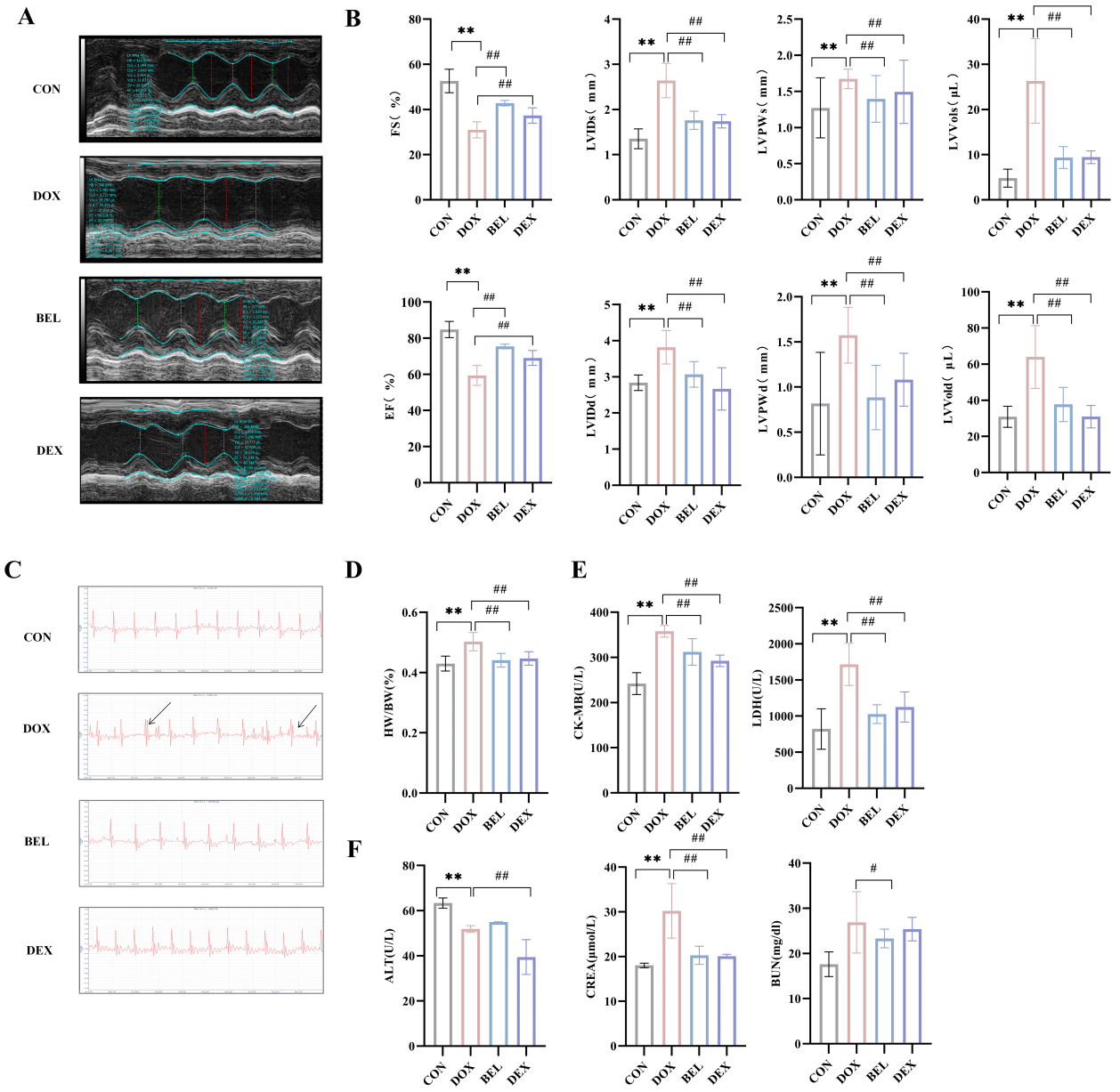

Fig. 1. Effects of bellidifolin (BEL) on cardiac function, myocardial injury, and hepatorenal damage in mice. (A) Echocardiography of mice. (B) Cardiac function indices of mice. (C) Electrocardiogram of mice (The area pointed to by the arrow corresponds to the electrocardiographic features of arrhythmia). (D) Heart weight ratio of mice. (E) Serum indices of myocardial injury. (F) Serum indices of hepatorenal damage. (Data presented as mean ± SD. n = 6. Control (CON) *vs.* Doxorubicin (DOX): $^{**}p < 0.01$. DOX *vs.* BEL, DOX *vs.* DEX: $^{\#}p < 0.05, ^{\#\#}p < 0.01$).

number of genes enriched in each entry, and the color of the circles corresponds to different *p*-value ranges.

3.4.4 KEGG Pathway Enrichment Analysis

Pathway enrichment analysis ($p \leq 0.01$) of 16 potential targets mapped to 107 pathways. Primary and secondary classification annotations were performed for each KEGG entry, as shown in Fig. 4E. The primary KEGG classifications included Human Diseases, Cellular Processes, Environmental Information Processing, and Organismal Systems. The horizontal axis represents the number of targets enriched in each pathway. Secondary KEGG entries with higher numbers of enriched targets among the 16 targets included Cancer: Overview and Cardiovascular Disease. Subsequently, the top 20 pathways were visualized in ascending order of *p*-values, as shown in Fig. 4F. The color of the bubbles represents the magnitude of the *p*-value, while the size of the bubbles reflects the number of target genes in the pathway.

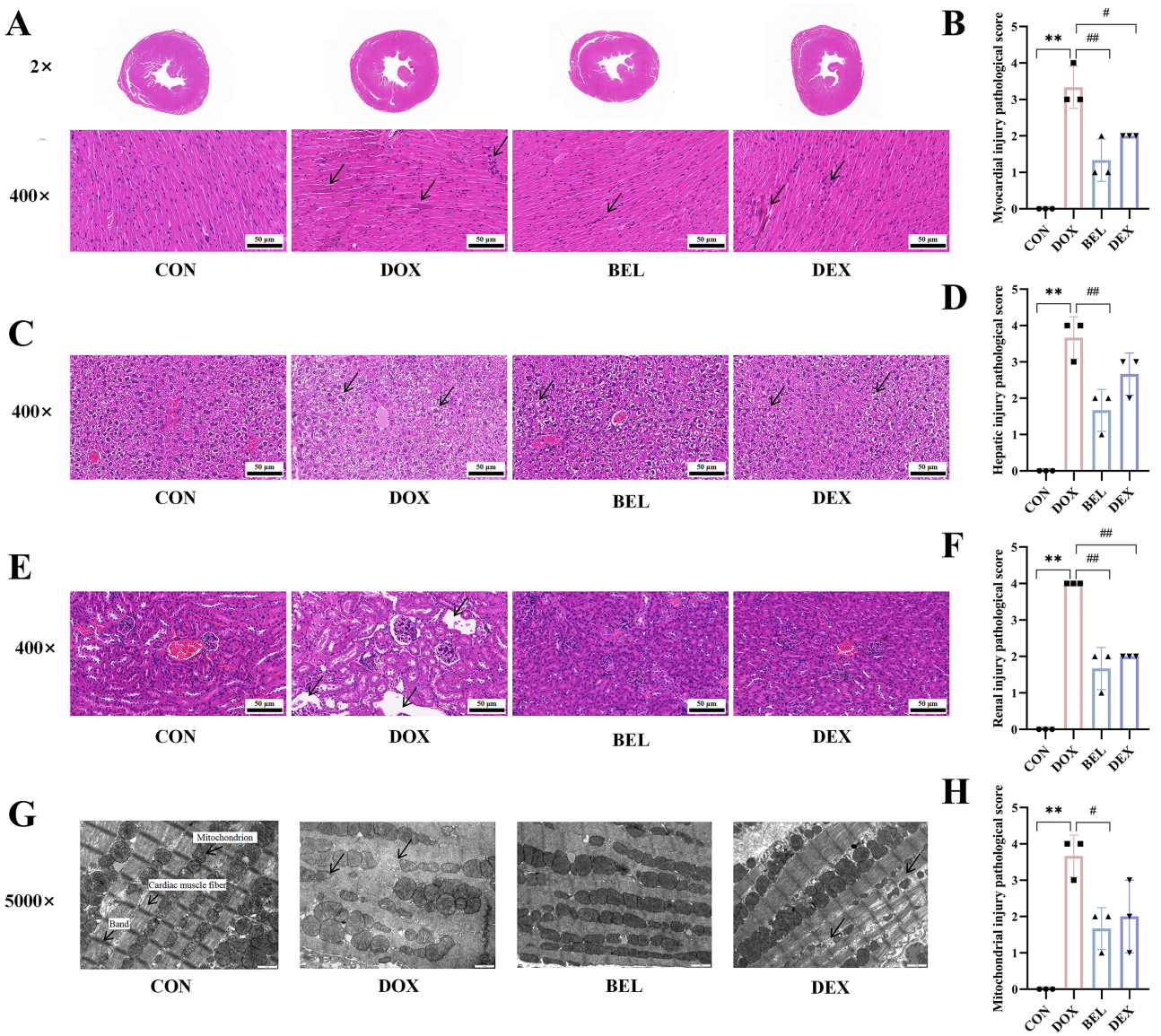

Fig. 2. BEL improves pathological changes in the myocardium, liver, and kidneys of cardiotoxic mice. (A,B) HE staining results of myocardial tissue (400×, The area pointed to by the black arrow corresponds to the region characterized by fibroblast proliferation and increased spacing between myocardial cells). Scale bar: 50 μm. (C,D) HE staining results of liver tissue (400×, The area pointed to by the black arrow corresponds to the region of hepatic steatosis). Scale bar: 50 μm. (E,F) HE staining results of renal tissue (400×, The area pointed to by the black arrow corresponds to the region characterized by renal cell necrosis and interstitial edema). Scale bar: 50 μm. (G,H) Ultrastructure of myocardial tissue (5000×, The area pointed to by the black arrow corresponds to the region characterized by mitochondrial disorganization and myofiber blurring). (CON *vs.* DOX: $^{**}p < 0.01$. DOX *vs.* BEL, DOX *vs.* DEX: $^{\#}p < 0.05$, $^{\#\#}p < 0.01$). Note: Pathological Scoring Criteria: (1) Myocardial Injury: Score 0: Myofibers are regularly arranged in bundles, with clear sarcomeres and neat alignment. Score 1: Scattered individual cells show vacuolation, myofibers are disorganized, and no obvious edema is present. Score 2: Myofiber fragmentation, partial inflammatory infiltration, and fibroblast proliferation are observed. Score 3: Extensive fibroblast proliferation, darkly stained cells, eosinophilic changes, and inflammatory infiltration are present. (2) Hepatic Injury: Score 0: No steatosis, no inflammatory cell infiltration, and no fibrosis. Score 1: Mild steatosis, inflammatory cell infiltration, and fibrosis. Score 2: Moderate steatosis, inflammatory cell infiltration, and fibrosis. Score 3: Severe steatosis, inflammatory cell infiltration, and fibrosis. (3) Renal Injury: Score 0: No cell necrosis and no interstitial edema. Score 1: Mild cell necrosis or interstitial edema. Score 2: Moderate cell necrosis or interstitial edema. Score 3: Severe cell necrosis or interstitial edema. (4) Mitochondrial Injury: Score 0: Mitochondria are neatly arranged, and myofibers are clear. Score 1: Mild disorganization of mitochondrial arrangement. Score 2: Disorganized mitochondrial arrangement and blurred myofibers. Score 3: Severe disorganization of mitochondrial size, structure, and arrangement, with blurred myofibers. Scale bar: 1 μm.

IMR Press

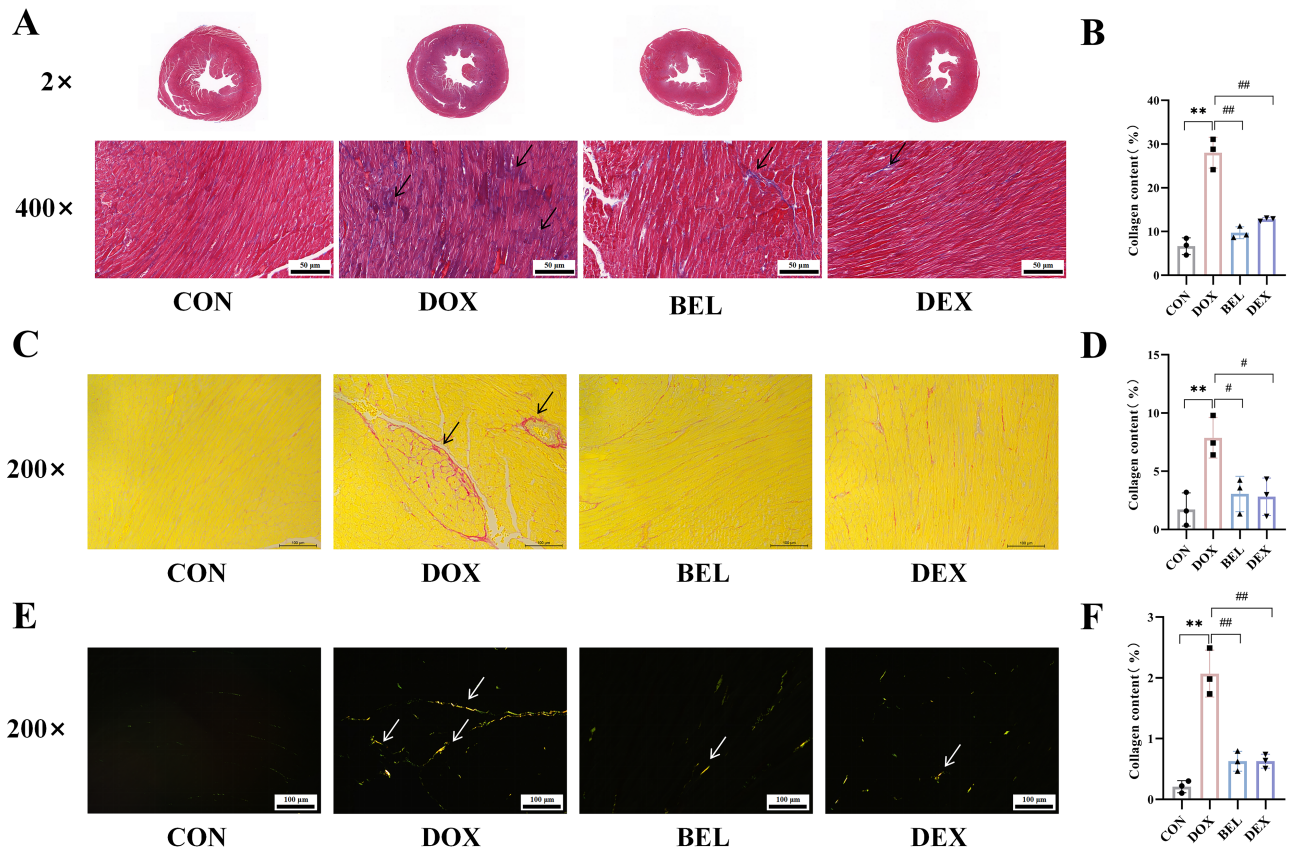

Fig. 3. BEL ameliorates myocardial fibrosis in cardiotoxic mice. (A,B) Masson staining results of myocardial tissue (400×, Collagen fibers: blue. muscle fibers: red. cell nuclei: blackish blue, the region denoted by the arrow corresponds to the area of collagen fiber deposition). Scale bar: 50 μm. (C,D) Sirius red staining of myocardial tissue (200×, Collagen fibers: red. muscle fibers: yellow, the region denoted by the arrow corresponds to the area of collagen fiber deposition). Scale bar: 100 μm. (E,F) Sirius red (polarized light) staining of myocardial tissue (200×, Collagen I: yellowish-red/orange-red. Collagen III: green, the region denoted by the arrow corresponds to the area of collagen fiber deposition). Scale bar: 100 μm. (CON *vs.* DOX: $^{**}p < 0.01$. DOX *vs.* BEL, DOX *vs.* DEX: $^{\#}p < 0.05$, $^{\#\#}p < 0.01$).

3.5 Molecular Docking Results

Molecular docking of BEL with the 16 core targets was performed to verify its binding capacity to target proteins at varying degrees. Based on the aforementioned criteria, the PDB files of AKT1 (7MYX), EGFR (8A27), BCL2 (8H7B), CASP3 (7JI7), STAT3 (6TLC), IL6 (5GW9), TNF (6U66), PTGS2 (5F19), CCND1 (6P8E), ESR1 (7UJO), HSP90AA1 (3O0I), SRC (3EAC), TGF-β1 (5VQP), HDAC1 (7Z1K), CDK2 (6Q4G), and CDK4 (7OXW) were selected for docking with BEL (Fig. 5). The results demonstrated that BEL satisfied the criteria for docking with the key targets. Details such as binding energy and binding site information are presented in Table 3, confirming that BEL intervenes in DIC through core targets.

3.6 Molecular Dynamics Simulation Results

Based on the molecular docking results, the TGF-β1-BEL complex was selected for molecular dynamics simulation to evaluate the binding stability of the protein-ligand complex. Fig. 6A illustrates the binding mode of the TGF-β1-BEL complex. The root-mean-square deviation (RMSD), a key indicator of conformational atomic deviations, was used to monitor the stability of the complex system. As shown in Fig. 6B, the RMSD of the TGF-β1-BEL complex stabilized between 50,000 and 100,000 ps, indicating minimal conformational changes in the TGF-β1 protein and relatively stable binding between TGF-β1 and BEL. The root-mean-square fluctuation (RMSF) reflects the flexibility of amino acid residues. Fig. 6C shows significantly higher flexibility in the amino acid residues between positions 180–220 and 300–340 of TGF-β1 in the TGF-β1-BEL complex compared to other regions. Fig. 6D presents the binding free energy calculated by the YASARA program, confirming that BEL binds stably to TGF-β1 with strong binding energy and affinity.

Fig. 4. Network pharmacology results of BEL intervention in doxorubicin-induced cardiotoxicity. (A) Venn diagram of intersections between BEL targets and cardiotoxicity targets. (B) PPI network diagram. (C) Bar chart of GO analysis. (D) Bubble chart of GO secondary analysis. (E) Bar chart of KEGG. (F) Bubble chart of KEGG.

Table 2. Topological parameters of key targets for BEL intervention in DIC.

Uniport ID	Protein target	Hub genes	Degree	Closeness	Betweenness
P31749	RAC-alpha serine/threonine-protein kinase	AKT1	48	0.8428571	207.92517
P00533	Epidermal growth factor receptor	EGFR	45	0.7972973	219.73232
P10415	Apoptosis regulator Bcl-2	BCL2	44	0.7972973	131.657
P42574	Caspase-3	CASP3	43	0.7763158	132.9298
P40763	Signal transducer and activator of transcription 3	STAT3	43	0.7866667	135.45213
P05231	Interleukin-6	IL6	42	0.7763158	122.438065
Q9UNG2	Tumor necrosis factor ligand superfamily member	TNF	42	0.7763158	121.26485
P35354	Prostaglandin G/H synthase 2	PTGS2	40	0.75641024	143.20937
P24385	G1/S-specific cyclin-D1	CCND1	38	0.72839504	145.6201
P03372	Estrogen receptor	ESR1	37	0.72839504	88.119705
P07900	Heat shock protein HSP 90-alpha	HSP90AA1	37	0.72839504	136.71877
P12931	Proto-oncogene tyrosine-protein kinase Src	SRC	36	0.7108434	55.051365
P01137	Transforming growth factor beta-1 proprotein	TGF-β1	35	0.70238096	153.86162
Q13547	Histone deacetylase 1	HDAC1	31	0.6781609	159.10611
P24941	Cyclin-dependent kinase 2	CDK2B1	28	0.64835167	108.45579
P11802	Cyclin-dependent kinase 4	CDK4	27	0.6413044	64.967896

Notes: Degree reflects the number of connections a node has, Betweenness measures the bridging role of a node within the shortest paths, Closeness represents the reciprocal of the average distance from the node to all other nodes. These three indicators are commonly used to assess the topological properties of each node. Higher values indicate more important nodes. Consequently, key targets were selected based on the criterion that all three indicators were higher than the average. AKT1, RAC-alpha serine/threonine-protein kinase; EGFR, Epidermal Growth Factor Receptor; BCL2, B-cell lymphoma 2; CASP3, Caspase-3; STAT3, Signal Transducer and Activator of Transcription 3; IL6, Interleukin 6; TNF, Tumor Necrosis Factor; PTGS2, Prostaglandin G/H synthase 2; CCND1, cyclin-D1; ESR1, Estrogen Receptor 1; HSP90AA1, Heat Shock Protein 90 Alpha Family Class A Member 1; SRC, Proto-oncogene tyrosine-protein kinase Src; TGF-β1, Transforming Growth Factor Beta 1; HDAC1, Histone Deacetylase 1; CDK2B1, Cyclin-dependent kinase 2B1; CDK4, Cyclin-Dependent Kinase 4.

Table 3. Molecular docking results of BEL and key target proteins.

	Vina scores	Cavity size	Center			Size		
			x	y	z	x	y	z
AKT1	–6.5	84	14	7	16	20	20	20
EGFR	–8.1	3691	18	–10	–13	30	28	31
BCL2	–7.0	3257	2	–1	–13	20	29	32
CASP3	–7.1	2136	3	3	–24	20	32	20
STAT3	–7.6	607	14	49	66	20	20	20
IL6	–8.0	669	–1	151	–5	20	20	20
TNF	–7.8	833	–41	105	–19	20	20	27
PTGS2	–9.3	1233	28	28	59	20	27	33
CCND1	–6.9	413	11	30	72	20	20	20
ESR1	–7.7	2644	12	–21	–24	20	32	20
HSP90AA1	–9.2	2115	–6	–10	–25	26	20	20
SRC	–6.1	54	–11	8	–5	20	20	20
TGF-β1	–6.8	198	97	54	52	20	20	20
HDAC1	–6.5	85	23	9	0	20	20	20
CDK2	–7.3	444	0	–7	–25	20	20	20
CDK4	–5.9	360	12	38	9	20	20	20

Notes: The Vina score is a scoring function used to evaluate the binding strength in molecular docking. It calculates the interaction and binding free energies between molecules to assign a score, with lower scores indicating stronger binding. A Vina score <-5.0 suggests potential binding activity, while a Vina score <-7.0 indicates stable docking between the protein and ligand.

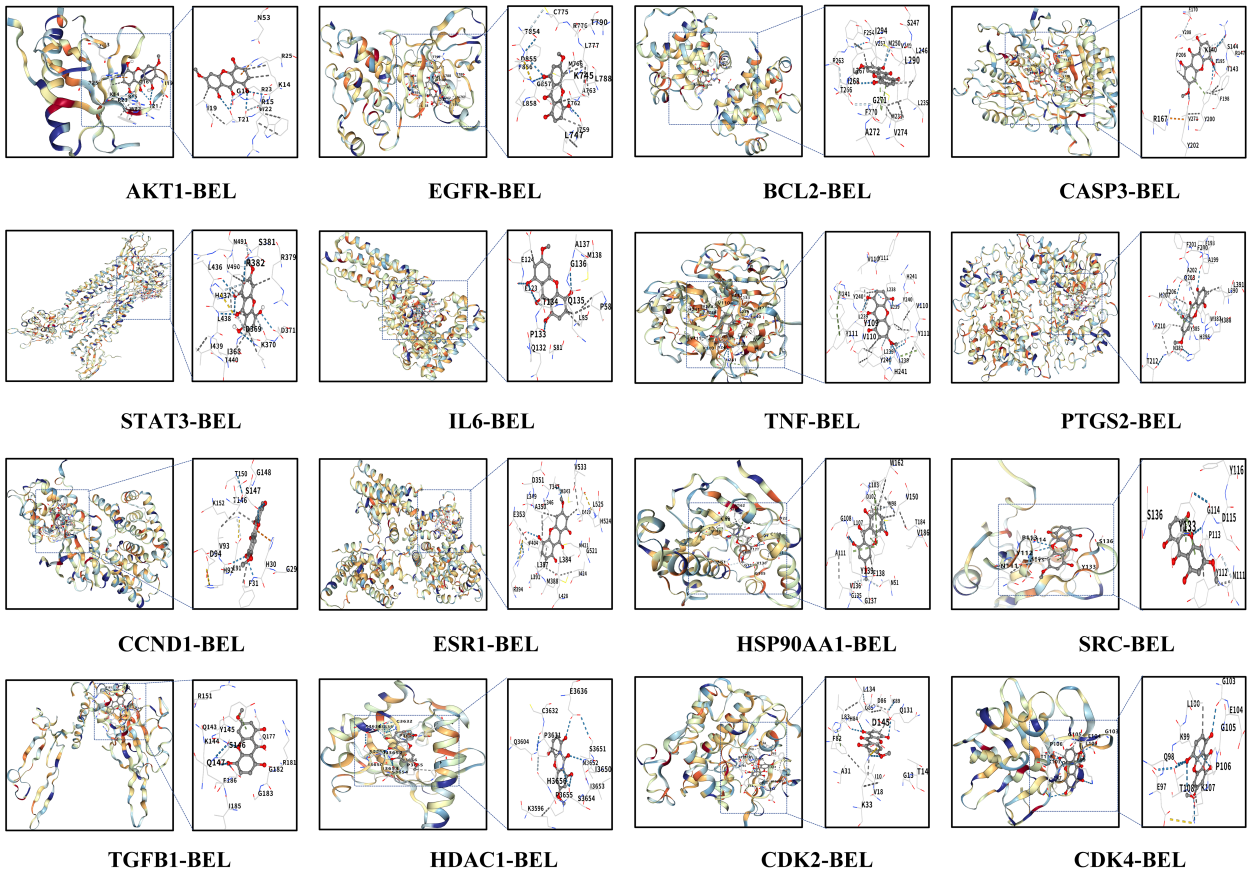

Fig. 5. Molecular docking results of BEL and key target proteins. Note: Hydrogen bonds (blue dotted line), weak hydrogen bonds (white dotted line), hydrophobic interactions (gray dotted line), ionic interactions (yellow dotted line), cation-π interactions (orange dotted line), and π-π stacking forces (green dotted line).

3.7 BEL Reduces the Expression of Fibrosis Markers by Regulating the TGF-β1 Target

The expression of TGF-β1 was assessed in different groups of mice *in vivo* using immunohistochemistry, RT-qPCR, and Western blotting (WB). Results showed a significant increase in TGF-β1 expression in the model group ($p < 0.01$), while all treatment groups exhibited a significant decrease in TGF-β1 levels ($p < 0.01$) (Fig. 7A–C). These results confirm that TGF-β1 is a key target for BEL in the treatment of DIC.

Following the same verification methods as for TGF-β1, the expression of fibrosis-related markers α-SMA, Col I, and Col III was further assessed at the tissue, protein, and gene levels. The results revealed a significant increase in α-SMA expression in the model group ($p < 0.01$), which was significantly reduced after intervention with BEL and DEX ($p < 0.01$) (Fig. 7D–F). The expression trends of Col I and Col III mirrored those of α-SMA (Fig. 7G–I).

3.8 BEL Ameliorates Myocardial Fibrosis by Regulating the PI3K-AKT Pathway

Given that TGF-β1 exerts its effects via regulation of the PI3K-AKT signaling pathway, which was also identified in the KEGG enrichment analysis (Fig. 3E), the expression of PI3K, AKT, and their phosphorylated forms in myocardial tissues was further investigated. The results showed that p-PI3K/PI3K and p-AKT/AKT were significantly decreased in the model group ($p < 0.01$), but were significantly restored after treatment with BEL and DEX ($p < 0.01$), as shown in Fig. 8.

4. Discussion

Extensive research indicates that DIC significantly raises the mortality risk of cancer patients, thus limiting its widespread clinical use [20,21]. As the global incidence of cancer continues to rise, DIC warrants greater attention. Early diagnosis and treatment of DIC are essential for improving clinical outcomes. However, current therapeutic options for DIC have limitations in addressing this complex condition [22]. This study aims to identify a potential therapeutic candidate for DIC and clarify its underlying mechanisms.

Network pharmacology analysis was employed in this study to explore the targets and mechanisms of BEL in the treatment of DIC. The results revealed 61 drug targets overlapping with DIC disease genes. Among these, 16 core tar-

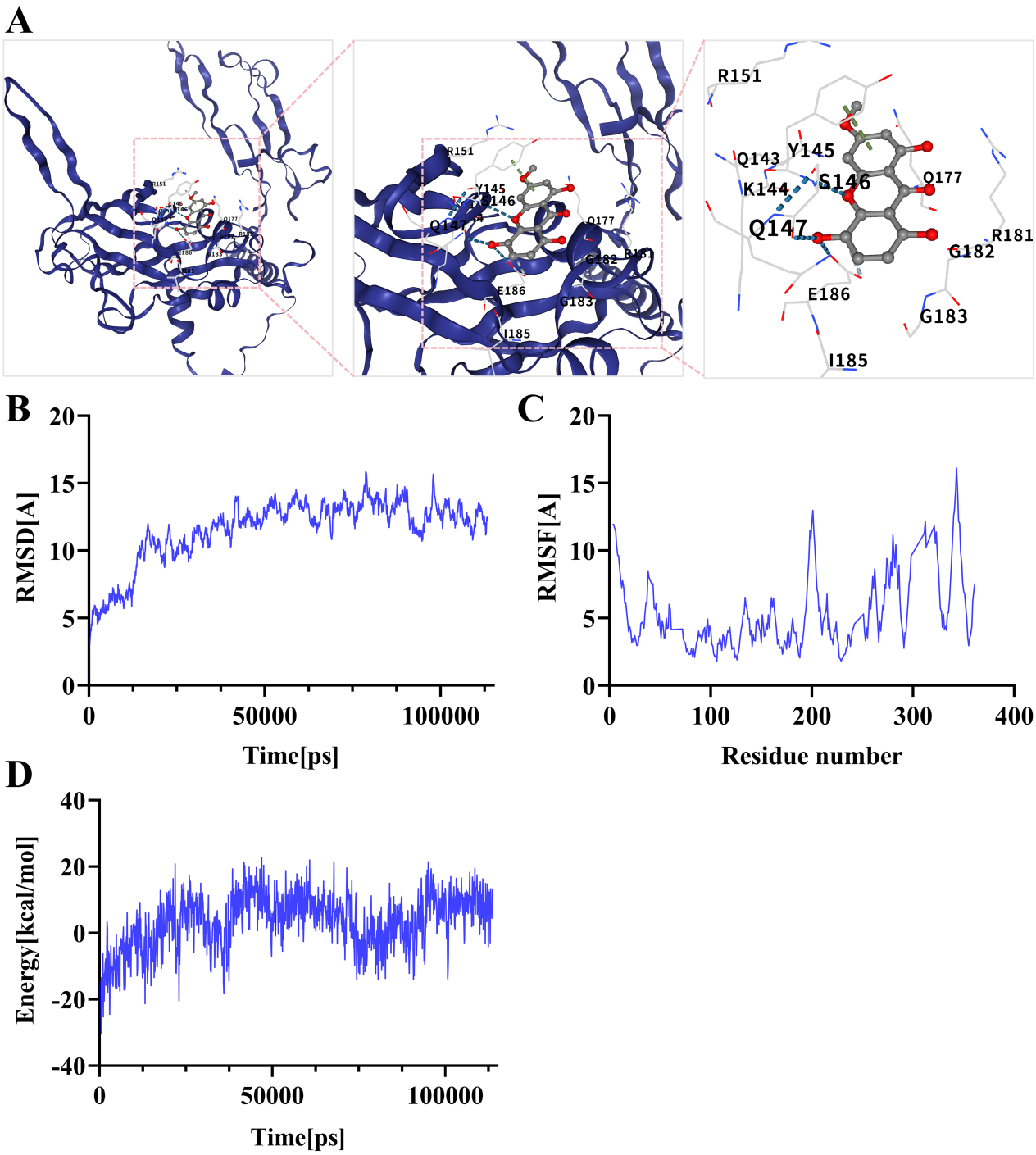

Fig. 6. Molecular dynamics simulation results of BEL and key target proteins. (A) Binding mode of the TGF-β1-BEL complex. (B) RMSD. (C) RMSF. (D) Binding energy.

gets were identified through PPI network analysis, including AKT, TGF-β1, and TNF. KEGG enrichment analysis indicated that these core targets were primarily involved in the PI3K-AKT signaling pathway, the TNF signaling pathway, and the IL-17 signaling pathway [23].

Chronic DIC is characterized by myocardial fibrosis, which significantly impairs cancer patient prognosis [24]. DIC leads to the upregulation of fibrosis markers, such as phospho-Smad3, collagen I, fibronectin, and α-SMA. BEL has been found to inhibit SOX9, blocking TGF-β1 signaling activation and ameliorating myocardial fibrosis [14]. Previous study confirmed that BEL improves myocardial fibrosis by inhibiting fibroblast activity [15]. *In vivo* experiments conducted in this study demonstrated that BEL can reduce collagen accumulation in myocardial tissue, showing cardioprotective effects comparable to DEX. Thus, in-

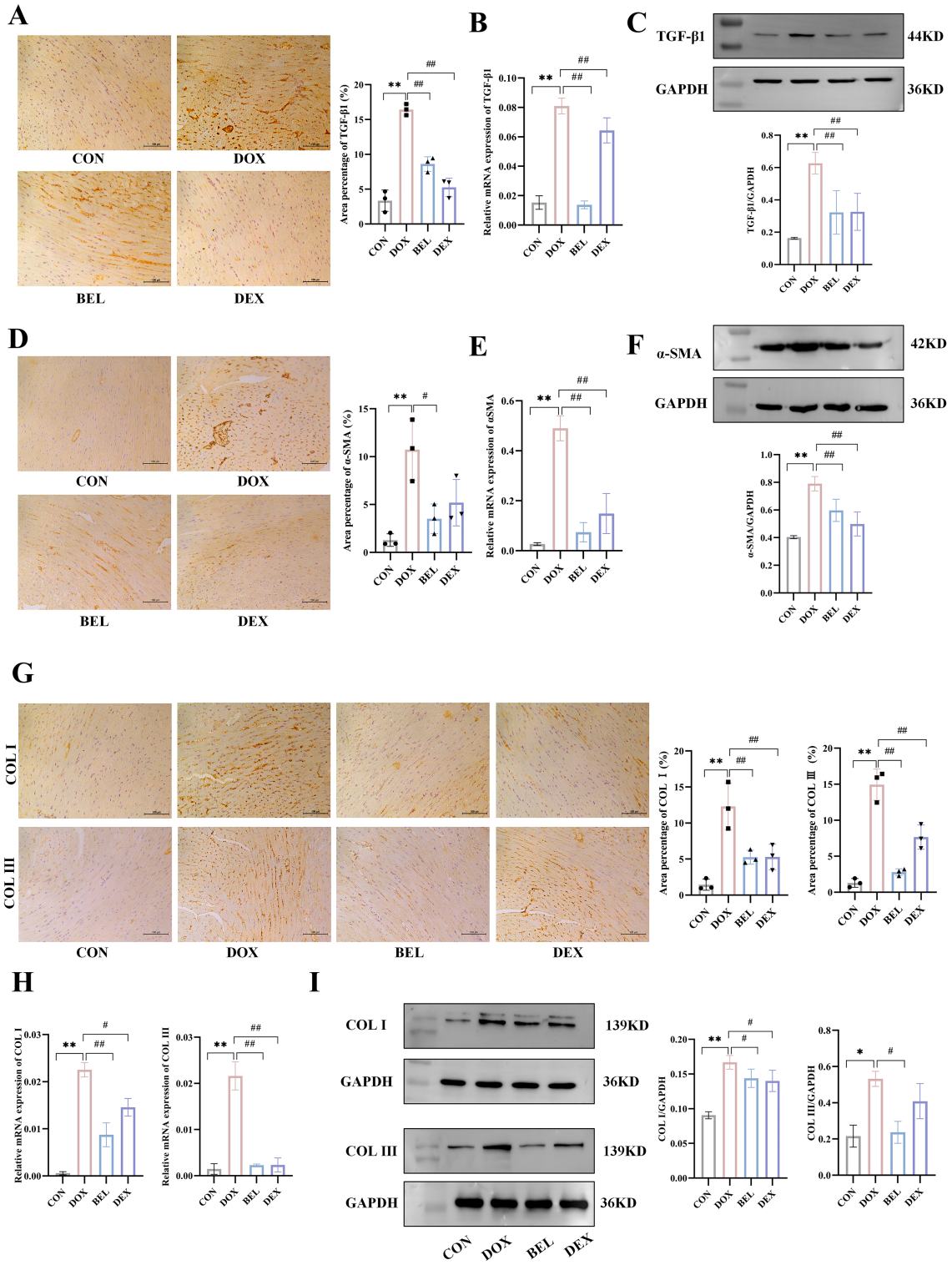

Fig. 7. Expression of TGF-β1, α-SMA, Col I, and Col III in myocardial tissue of mice. (A) Immunohistochemical detection of TGF-β1 (200×). Scale bar: 100 μm. (B) RT-qPCR detection of TGF-β1. (C) Western blotting detection and grayscale analysis of TGF-β1. (D) Immunohistochemical detection of α-SMA (200×). Scale bar: 100 μm. (E) RT-qPCR detection of α-SMA. (F) WB detection and grayscale analysis of α-SMA. (G) Immunohistochemical detection of Col I and Col III (200×). Scale bar: 100 μm. (H) RT-qPCR detection of Col I and Col III. (I) WB detection and grayscale analysis of Col I and Col III. (Antibody dilution: TGF-β1 = 1:20,000. α-SMA = 1:5000. Col I = 1:1000. Col III = 1:1000) (CON *vs.* DOX: $^{*}p < 0.05$, $^{**}p < 0.01$. DOX *vs.* BEL, DOX *vs.* DEX: $^{\#}p < 0.05$, $^{\#\#}p < 0.01$).

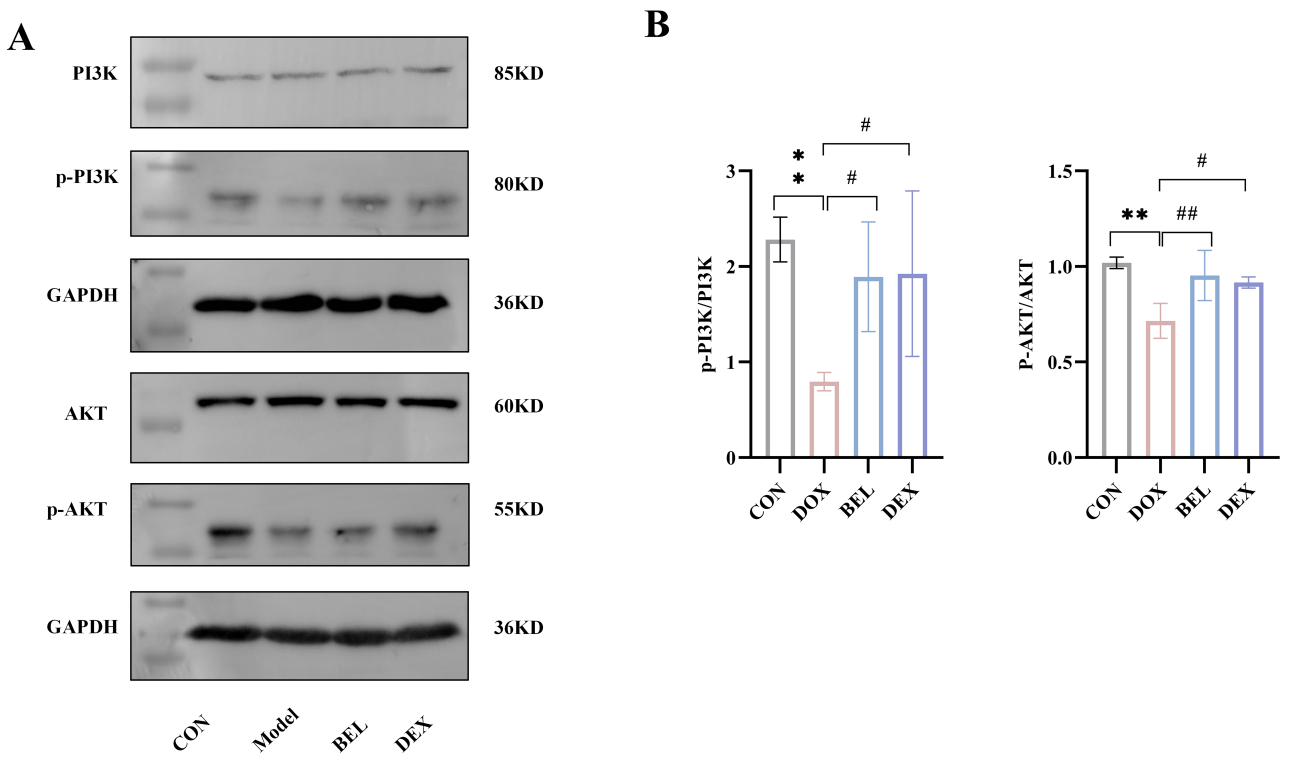

Fig. 8. Expression of the PI3K-AKT signaling pathway in myocardial tissue of mice. (A) WB detection strip chart. (B) Grayscale analysis of WB detection. (Antibody dilution: PI3K = 1:1000. p-PI3K = 1:1000. AKT = 1:1000. p-AKT = 1:1000) (CON *vs.* DOX: $^{*}p < 0.05$, $^{**}p < 0.01$. DOX *vs.* BEL, DOX *vs.* DEX: $^{\#}p < 0.05$, $^{\#\#}p < 0.01$).

hibition of collagen accumulation-mediated myocardial fibrosis could be a key pathway through which BEL exerts its therapeutic effects in DIC. In conclusion, TGF-β1 appears to be a potential target for BEL in treating DIC.

TGF-β1 is a multifunctional cytokine that modulates multiple cellular processes, such as inflammation, extracellular matrix deposition, and cell proliferation, differentiation, and growth [25]. It exerts a key regulatory effect on fibroblast phenotype and function [26,27]. TGF-β1 stimulation promotes myofibroblast differentiation and upregulates the synthesis of extracellular matrix proteins. Additionally, TGF-β1 is a powerful inducer of CTGF—a fibrogenic mediator that cooperates with TGF-β1 to facilitate sustained fibrosis [28]. Emerging research indicates that the fibrogenic actions of TGF-β1, as opposed to its anti-inflammatory effects, are transduced via the PI3K/Akt signaling pathway [29].

Numerous studies have confirmed that the PI3K/Akt signaling pathway plays a key role in regulating the development, progression, and pathological formation of cardiac fibrosis by modulating cell survival, apoptosis, proliferation, myocardial contractility, and the transcription of associated genes, involving molecules such as mTOR, GSK-3, FoxO1/3, and NOS [30–32]. This study demonstrates that both BEL and DEX reduce collagen accumulation in myocardial tissue by regulating the PI3K-AKT signaling pathway. Additionally, TEM results revealed damage to the myocardial mitochondria in the model group, which may be attributed to oxidative stress and mitochondrial dysfunction—key pathogenic mechanisms of DIC. Both BEL and DEX were found to improve mitochondrial structure, providing another potential pathway for their cardioprotective effects.

Based on these findings, it can be inferred that BEL treats DIC by inhibiting myocardial fibrosis. The strength of this study lies in its identification of the potential mechanisms of DIC through network pharmacology analysis and the provision of a promising therapeutic drug. Future studies will focus on determining the optimal human dosage of BEL, evaluating its potential interactions with chemotherapeutic drugs, and conducting safety assessments to provide a solid foundation for its clinical application.

5. Conclusion

In this study, the primary mechanism by which BEL treats DIC appears to be its anti-myocardial fibrosis effect, with TGF-β and the PI3K-AKT pathway identified as potential key targets and pathways. However, due to the limitations of this study, further investigations will explore BEL's cardioprotective effects in other cardiotoxicity models or tumor models. These efforts are expected to deepen our understanding of the mechanisms involved and contribute to drug development for DIC.

6. Limitations

This study has several limitations: First, the *in vivo* drug metabolism of BEL remains unclear. Second, additional cellular experiments are needed to verify the biological functional modules involved. Third, while a 4-week acute animal model was used, DIC may occur years after treatment in clinical settings. Therefore, future research will focus on establishing a chronic DIC model to investigate the long-term effects of BEL. Fourth, only male mice were used, and future studies will examine potential differences in the ameliorative effects of BEL in female mice. Fifth, the timing of BEL administration in this study was aligned with the modeling period. however, further investigation is needed to explore the effects of pre-modeling versus post-modeling administration. Sixth, the effect of BEL on tumor cells and its potential interference with the antitumor efficacy of DOX remain unclear. Seventh, pathway inhibition experiments and small interfering RNA (siRNA) experiments targeting the TGF-β1 and PI3K/AKT pathways were not conducted, making it impossible to distinguish whether BEL's effects on these pathways are direct or secondary. These issues will be further explored in subsequent studies.

Availability of Data and Materials

The authors confirm that the data supporting the findings of this study are available within the article. The data associated with this paper are available upon request to the corresponding author.

Author Contributions

Conceptualization: XMZ, YL, AYL; Data curation: XMZ, AYL; Formal analysis: CD, AYL; Funding acquisition: YL, AYL; Investigation: XMZ; Methodology: XMZ, FG, YL; Project administration: YL, AYL; Resources: JLW; Software: ZYZ, FG; Supervision: JLW; Validation: XMZ; Visualization: XMZ, YLL; Writing—original draft: XMZ, ZYZ, AYL; Writing—review and editing: YL, AYL. All authors contributed to editorial changes in the manuscript. All authors read and approved the final manuscript. All authors have participated sufficiently in the work and agreed to be accountable for all aspects of the work.

Ethics Approval and Consent to Participate

The animal study protocol was approved by the Animal Welfare Committee of Hebei University of Chinese Medicine (Approval No.: DWLL202212032). The study adhered to the guidelines set by the committee.

Acknowledgment

The authors would like to express our gratitude to all those who helped me during the writing of this manuscript. And thanks to all the peer reviewers for their opinions and suggestions.

Funding

This work was supported by the Hebei Natural Science Foundation [grant number: H2025423167]; the National Natural Science Foundation Youth Fund of China [grant number: 81500317].

Conflict of Interest

The authors declare no conflict of interest.

References

[1] Li X. Doxorubicin-mediated cardiac dysfunction: Revisiting molecular interactions, pharmacological compounds and (nano)theranostic platforms. Environmental Research. 2023; 234: 116504. https://doi.org/10.1016/j.envres.2023.116504.

[2] Kalyanaraman B. Teaching the basics of the mechanism of doxorubicin-induced cardiotoxicity: Have we been barking up the wrong tree? Redox Biology. 2020; 29: 101394. https://doi.org/10.1016/j.redox.2019.101394.

[3] Jones IC, Dass CR. Doxorubicin-induced cardiotoxicity: causative factors and possible interventions. The Journal of Pharmacy and Pharmacology. 2022; 74: 1677–1688. https://doi.org/10.1093/jpp/rgac063.

[4] Pawar HD, Dusane S, Sharma T, Nakhate KT, Goyal SN. Doxorubicin-Induced Cardiotoxicity: Exploration of Molecular Pathogenesis and Phytocompound-Based Therapeutic Strategies. Current Pharmaceutical Design. 2025. https://doi.org/10.2174/0113816128410093251006160508. (Online ahead of print)

[5] de Baat EC, Mulder RL, Armenian S, Feijen EA, Grotenhuis H, Hudson MM, *et al*. Dexrazoxane for preventing or reducing cardiotoxicity in adults and children with cancer receiving anthracyclines. The Cochrane Database of Systematic Reviews. 2022; 9: CD014638. https://doi.org/10.1002/14651858.CD014638.pub2.

[6] Goey AKL, Schellens JHM, Beijnen JH, Huitema ADR. Dexrazoxane in anthracycline induced cardiotoxicity and extravasation. Nederlands Tijdschrift Voor Geneeskunde. 2010; 154: A1155.

[7] Zhou D, Liu W, Zhang J, Dong Y, Wu J, Zhang Y, *et al*. Bellidifolin ameliorates isoprenaline-induced cardiac hypertrophy by the Nox4/ROS signalling pathway through inhibiting BRD4. Cell Death Discovery. 2023; 9: 279. https://doi.org/10.1038/s41420-023-01563-2.

[8] Ge H, Du Z, Liu W, Wang L, Li J, Yang G, *et al*. Gen-miR-5 derived from *Gentianella acuta* inhibits PFKP to prevent fibroblast activation and alleviate myocardial fibrosis. Frontiers in Pharmacology. 2025; 16: 1578877. https://doi.org/10.3389/fphar.2025.1578877.

[9] Wei Y, Wang Y, Jiang X, Sun Y, Wang M, Wang Z, *et al*. Xanthones explore the mechanism of p53/p21 signaling pathway to prevent cardiac aging and epigenetic regulation of Nrf2 gene. Archives of Gerontology and Geriatrics. 2025; 236: 116878. https://doi.org/10.1016/j.archger.2025.105759.

[10] Dai C, Sun J, Yang G, Zhang C, Zhang Y, Song Q, *et al*. The total xanthones from Gentianella acuta alleviate acute myocardial infarction by targeting BRD4-mediated cardiomyocyte pyroptosis and inflammation. Phytomedicine: International Journal of Phytotherapy and Phytopharmacology. 2025; 147: 157156. https://doi.org/10.1016/j.phymed.2025.157156.

[11] Zhou WW, Dai C, Liu WZ, Zhang C, Zhang Y, Yang GS, *et al*. Gentianella acuta improves TAC-induced cardiac remodelling by regulating the Notch and PI3K/Akt/FOXO1/3 pathways. Biomedicine & Pharmacotherapy = Biomedecine & Phar-

macotherapie. 2022; 154: 113564. https://doi.org/10.1016/j.biopha.2022.113564.

[12] Si M, Wu M, Huo Y, Li A, Guan S, Ma D, *et al*. *Gentianella acuta* mitigates cardiovascular damage and inflammation in diet-induced hypercholesterolaemic rats. Experimental and Therapeutic Medicine. 2021; 22: 1259. https://doi.org/10.3892/etm.2021.10694.

[13] Gao F, Chen Z, Zhou L, Xiao X, Wang L, Liu X, *et al*. Preparation, characterization and *in vitro* study of bellidifolin nanomicelles. RSC Advances. 2022; 12: 21982–21989. https://doi.org/10.1039/d2ra02779h.

[14] Yao TT, Yang HX, Sun JH, Zhang Y, Zhang Y, Song QH, *et al*. Bellidifolin Inhibits SRY-Related High Mobility Group-Box Gene 9 to Block TGF-β Signalling Activation to Ameliorate Myocardial Fibrosis. Evidence-based Complementary and Alternative Medicine: ECAM. 2022; 2022: 6841276. https://doi.org/10.1155/2022/6841276.

[15] Yang HX, Sun JH, Yao TT, Li Y, Xu GR, Zhang C, *et al*. Bellidifolin Ameliorates Isoprenaline-Induced Myocardial Fibrosis by Regulating TGF-β1/Smads and p38 Signaling and Preventing NR4A1 Cytoplasmic Localization. Frontiers in Pharmacology. 2021; 12: 644886. https://doi.org/10.3389/fphar.2021.644886.

[16] Zhao L, Zhang H, Li N, Chen J, Xu H, Wang Y, *et al*. Network pharmacology, a promising approach to reveal the pharmacology mechanism of Chinese medicine formula. Journal of Ethnopharmacology. 2023; 309: 116306. https://doi.org/10.1016/j.jep.2023.116306.

[17] Dos Santos Nascimento IJ, de Moura RO. Molecular Dynamics Simulations in Drug Discovery. Mini Reviews in Medicinal Chemistry. 2024; 24: 1061–1062. https://doi.org/10.2174/1389557524112404021347 19.

[18] Ma YL, Huo XW, Wong C, Zhou FJ, Li SZ, Zhang H, *et al*. Salvianolic acid A targets glutamic-oxaloacetic transaminase 2 to ameliorate doxorubicin-induced myocardial oxidative injury by activating malate-aspartate NADH shuttle. Phytomedicine: International Journal of Phytotherapy and Phytopharmacology. 2025; 148: 157492. https://doi.org/10.1016/j.phymed.2025.157492.

[19] Curran CF, Narang PK, Reynolds RD. Toxicity profile of dexrazoxane (Zinecard, ICRF-187, ADR-529, NSC-169780), a modulator of doxorubicin cardiotoxicity. Cancer Treatment Reviews. 1991; 18: 241–252. https://doi.org/10.1016/0305-7372(91)90015-r.

[20] Xu A, Deng F, Chen Y, Kong Y, Pan L, Liao Q, *et al*. NF-κB pathway activation during endothelial-to-mesenchymal transition in a rat model of doxorubicin-induced cardiotoxicity. Biomedicine & Pharmacotherapy = Biomedecine & Pharmacotherapie. 2020; 130: 110525. https://doi.org/10.1016/j.biopha.2020.110525.

[21] Herrmann J. Adverse cardiac effects of cancer therapies: cardiotoxicity and arrhythmia. Nature Reviews. Cardiology. 2020; 17: 474–502. https://doi.org/10.1038/s41569-020-0348-1.

[22] Sheibani M, Azizi Y, Shayan M, Nezamoleslami S, Eslami F, Farjoo MH, *et al*. Doxorubicin-Induced Cardiotoxicity: An Overview on Pre-clinical Therapeutic Approaches. Cardiovascular Toxicology. 2022; 22: 292–310. https://doi.org/10.1007/s12012-022-09721-1.

[23] Zhu Y, Zhang Q, Wang Y, Liu W, Zeng S, Yuan Q, *et al*. Identification of Necroptosis and Immune Infiltration in Heart Failure Through Bioinformatics Analysis. Journal of Inflammation Research. 2025; 18: 2465–2481. https://doi.org/10.2147/JIR.S502203.

[24] Huyan Y, Chen X, Chang Y, Hua X, Fan X, Shan D, *et al*. Single-Cell Transcriptomic Analysis Reveals Myocardial Fibrosis Mechanism of Doxorubicin-Induced Cardiotoxicity. International Heart Journal. 2024; 65: 487–497. https://doi.org/10.1536/ihj.23-302.

[25] Dobaczewski M, Chen W, Frangogiannis NG. Transforming growth factor (TGF)-β signaling in cardiac remodeling. Journal of Molecular and Cellular Cardiology. 2011; 51: 600–606. https://doi.org/10.1016/j.yjmcc.2010.10.033.

[26] Mauviel A. Transforming growth factor-beta: a key mediator of fibrosis. Methods in Molecular Medicine. 2005; 117: 69–80. https://doi.org/10.1385/1-59259-940-0:069.

[27] Li WQ, Tan SL, Li XH, Sun TL, Li D, Du J, *et al*. Calcitonin gene-related peptide inhibits the cardiac fibroblasts senescence in cardiac fibrosis via up-regulating klotho expression. European Journal of Pharmacology. 2019; 843: 96–103. https://doi.org/10.1016/j.ejphar.2018.10.023.

[28] Leask A, Abraham DJ. TGF-beta signaling and the fibrotic response. FASEB Journal: Official Publication of the Federation of American Societies for Experimental Biology. 2004; 18: 816–827. https://doi.org/10.1096/fj.03-1273rev.

[29] Fu S, Song X, Hu Y, Zhu Q, Lv X, Tang X, *et al*. Neotuberostemonine and tuberostemonine ameliorate pulmonary fibrosis through suppressing TGF-β and SDF-1 secreted by macrophages and fibroblasts via the PI3K-dependent AKT and ERK pathways. Chinese Journal of Natural Medicines. 2023; 21: 527–539. https://doi.org/10.1016/S1875-5364(23)60444-3.

[30] Hsieh PL, Chu PM, Cheng HC, Huang YT, Chou WC, Tsai KL, *et al*. Dapagliflozin Mitigates Doxorubicin-Caused Myocardium Damage by Regulating AKT-Mediated Oxidative Stress, Cardiac Remodeling, and Inflammation. International Journal of Molecular Sciences. 2022; 23: 10146. https://doi.org/10.3390/ijms231710146.

[31] Wang D, Jin Y, Yang M, Xue Y, Zhang X, Guo Y, *et al*. Cardioprotective effect of *Saussurea involucrata* injection against Doxorubicin-induced cardiotoxicity by network pharmacology analysis and experimental verification. Acta Biochimica et Biophysica Sinica. 2024; 57: 554–568. https://doi.org/10.3724/abbs.2024170.

[32] Qin W, Cao L, Massey IY. Role of PI3K/Akt signaling pathway in cardiac fibrosis. Molecular and Cellular Biochemistry. 2021; 476: 4045–4059. https://doi.org/10.1007/s11010-021-04219-w.